

Chandra High Energy Transmission Grating Spectroscopy of Galactic Microquasar XTE J1550-564 in Outburst

J. M. Miller¹, H. L. Marshall¹, R. Wijnands^{1,8}, T. Di Matteo^{2,8},
 D. W. Fox¹, J. Kommers¹, D. Pooley¹, T. Belloni³, J. Casares⁴
 P. A. Charles⁵, A. C. Fabian⁶, M. van der Klis⁷, W. H. G. Lewin¹

Subject headings: Black hole physics – accretion – line:profiles – relativity – X-rays:bursts – X-rays:stars

ABSTRACT

We report the results of two *Chandra* X-ray Observatory High Energy Transmission Grating Spectrometer observations, made shortly after peak X-ray luminosity during the May, 2000 outburst of galactic microquasar XTE J1550–564. The observations were separated by 2.5 days. Nearly simultaneous observations were made with the *Rossi* X-ray Timing Explorer. We constrain the X-ray continuum emission in the region of the iron K_{α} line in the *Chandra* data via the results of fits to the *RXTE* data. The high-resolution *Chandra* spectra are featureless, with the possible exception of features at 6.7 keV and 7.0 keV (likely helium-like and hydrogenic iron, respectively). The *Chandra* spectra do allow but do not require a broad line component in the iron K_{α} region. We discuss these findings within the context of the general relativistic region around black holes and the accretion flow geometry of XTE J1550–564.

1. Introduction

The X-ray light curves of black hole (candidate) X-ray binary (BHC) systems are usually discussed in terms of canonical spectral and timing states. The physical environments in these systems are extreme: accreting matter is heated to become more luminous in optical bands than the companion star (Chen, Shrader, & Livio 1997), emission lines produced near

the black hole may be skewed by Doppler shifts and gravitational redshifts (Balucinska-Church & Church 2000, Miller et al. 2001), and matter may be expelled in collimated, polar, radio-bright jets at velocities exceeding $0.9c$ (Fender et al. 1999). Yet, the same distinct states are nonetheless observed in all such systems, whether transient or persistent. That this consistency is seen in such extreme environments has

¹Center for Space Research and Department of Physics, Massachusetts Institute of Technology, Cambridge, MA 02139–4307; jmm@space.mit.edu, rudy@space.mit.edu, derekfox@space.mit.edu, davep@space.mit.edu, hermanm@space.mit.edu, kommers@space.mit.edu, lewin@space.mit.edu

²Harvard–Smithsonian Center for Astrophysics, Harvard University, Cambridge MA 02138; tdimatte@cfa.harvard.edu

³Osservatorio di Brera, via Brera 28, Milano, I-20121, Italy; belloni@merate.mi.astro.it

⁴Instituto de Astrofísica de Canarias, 38200 La Laguna, Tenerife, Spain; jcv@ll.iac.es

⁵University of Southampton, SO17 1BJ, Southampton, UK; pac@astro.soton.ac.uk

⁶Cambridge University, Institute of Astronomy, Madingley Rd., Cambridge CB2 OHA U.K., acf@ast.cam.ac.uk

⁷Astronomical Institute 'Anton Pannekoek,' University of Amsterdam, and Center for High Energy Astrophysics, Kruislaan 403, 1098 SJ, Amsterdam, the Netherlands, michiel@astro.uva.nl

⁸*Chandra* fellow

fueled research to determine how, or indeed *if* the accretion flow geometry of these systems changes to produce the observed states.

Although several models have been fit to BHC spectra with similarly good statistical results, the spectra are usually fit with two components: the soft (<3 keV), quasi-thermal spectrum is fit with the multicolor disk blackbody model of Mitsuda et al. (1984), and the hard, higher-energy spectrum is fit with a simple power-law. The multicolor disk blackbody component models thermal emission from a geometrically-thin, optically thick disk of accreting matter, in which the temperature falls as a function of radius. The power-law component is thought to arise by inverse Compton processing (so-called Compton-upscattering, or Comptonization) of soft seed photons in an optically-thin region, perhaps located centrally or above the accretion disk (Sunyaev & Titarchuk, 1980). The multicolor disk blackbody component is characterized by the color “temperature” (kT), and the power-law by the photon index (α_{pl}). The relative flux contributed by these components in the 1–10 keV range, in combination with any observed rapid X-ray variability (such as broad band-limited noise or quasi-periodic oscillations – QPOs), define the canonical BHC states. In order of decreasing mass accretion rate, these states are: the very high state (VHS), high state (HS), intermediate state (IS), low state (LS), and quiescent (or, “off”) state (QS). These states and their particulars are discussed extensively in the literature (for a review, see, e.g. Tanaka & Lewin 1995). Homan et al. (2001), however, note that the state transitions in the 1998 outburst of XTE J1550–564 cannot be driven by the mass accretion rate alone.

Beyond the inferences of X-ray continuum measurements and variability analysis, line-resolved spectroscopy can provide a concrete and independent means of probing the inner accretion flow geometry in BHC systems. Emission lines may be shaped by a combination of Doppler shifting and gravitational redshifting. Each effect can be used to constrain the proximity of the emitting region to the black hole. Fabian et al. (1989) first

calculated how an iron K_{α} emission line might be shaped if formed in an accretion disk around a black hole; evidence of a redshifted $\text{Fe } K_{\alpha}$ line in Seyfert-1 galaxy MCG 6-30-15 (Tanaka et al. 1995) confirmed these calculations. Recent work has revealed evidence of $\text{Fe } K_{\alpha}$ lines shaped by combinations of gravitational redshifts and Doppler shifts in BHCs, and even suggested possible Kerr geometries (see, e.g., Balucinska-Church & Church 2000, Miller et al. 2001).

Apart from probing relativistic regimes, spectral emission and absorption lines may also reveal parameters like the ionization state, temperature, metallicity, and optical depth of the accreting plasma, and circumstellar envelope. Esin et al. (2001) note the possibility of a partially ionized circumsystemic gas in a *Chandra* LETG observation of BHC XTE J1118+480 (McClintock et al. 2001).

It is within the context of ascertaining the particulars of BHC accretion flow geometry, probing for relativistic effects in the extreme gravitational environment, and examining the possibility of a warm-absorber region in BHCs via line-resolved spectroscopy, that we have studied XTE J1550–564 with the High Energy Transmission Grating Spectrometer (HETGS) aboard *Chandra*. In the following sections, we summarize the outburst history of XTE J1550–564, and describe our observations. We detail our observational parameters, our analysis methods, and discuss our results within the context of the accretion environments found in other BHC systems.

2. Outburst History

XTE J1550–564 was discovered on 7 September 1998 (Smith 1998), by the *All Sky Monitor* (ASM) aboard the *Rossi X-ray Timing Explorer* (RXTE). A radio (Campbell-Wilson et al. 1998) and optical counterpart (Orosz, Bailyn, & Jain 1998) was quickly identified. The ensuing outburst lasted until June 1999, and displayed some of the most remarkable behavior yet seen in an X-ray nova, e.g. an initial flare which reached a flux level equivalent

to 6.8 Crab (1.5–12 keV, *RXTE*/ASM), very rapid state transitions, and strong (7% rms) QPOs at frequencies as high as 285 Hz (Sobczak et al. 2000, Homan et al. 2001).

An optically-determined mass function is the most certain method of classifying an X-ray nova as a BHC, as it is generally accepted that $\sim 3M_{\odot}$ is the upper-limit for a neutron star mass. Yet, even without a mass function, many X-ray novae are called BHCs if they display canonical X-ray spectral and timing states (described above) within their outburst light curve. On this basis, XTE J1550–564 was quickly identified as a BHC. Monitoring of the radio flux from XTE J1550–564 revealed optically thick emission, with apparent superluminal motion ($v_{\text{jet}} > 2c$) (Hannikainen et al. 2000). As a result, XTE J1550–564 was further classified as a “microquasar,” a term referring to the mass difference between the black holes inferred in BHCs ($\sim 10M_{\odot}$) and those thought to power Active Galactic Nuclei (AGN; 10^7 – 10^9M_{\odot}), which are also known to have strong, radio-bright jets. At the time, this class of objects included GRS 1915+105, GRO J1655–40, and CI Cam. Presently, this class includes these sources and XTE J1748–288, V4641 Sgr, SS 433, and possibly also XTE J1859+226, 4U 1630–472, and LS 5039.

On 2 April, 2000, new source activity was noticed by the *RXTE* ASM (Smith et al. 2000). XTE J1550–564 was active in X-rays for nearly 70 days thereafter, and reached a peak flux of ~ 1 Crab (ASM, 1.5–12 keV); it was also seen out to 300 keV with BATSE aboard *CGRO*, and simultaneously in optical bands (Masetti & Soria 2000, Jain & Bailyn 2000). Spectrally-inverted radio emission, likely from a compact jet, is detected in the LS, as well as a possible discrete ejection event at the LS–IS transition (Corbel et al. 2001). The ASM light curve and $(5\text{--}12 \text{ keV})/(3\text{--}5 \text{ keV})$ hardness ratio of this outburst is shown in Figure 1. The lightcurve of the first outburst of XTE J1550–564 departed radically from a typical profile (Homan et al. 2001), but the second outburst is similar to a fast-rise exponential-decay (or, “FRED”) envelope.

On 28 January, 2001, *RXTE* found XTE J1550–564 to be in the LS, with timing noise of 40% rms and a spectrum well-described by a power-law with $\alpha_{\text{pl}} = 1.52$ (Tomsick et al. 2001).

3. Observation and Analysis

The second outburst of XTE J1550–564 met the trigger criteria for our approved *Chandra* AO-1 target of opportunity (TOO) program, as well as our *RXTE* AO-5 TOO program. In all, we made seven observations of XTE J1550–564 with *Chandra* (18 observations with *RXTE*). Of these, here we report on the iron K_{α} region in the first two observations only (see Table 1), when the source is brightest. Lower energy spectral results from these *Chandra* observations, and spectral and timing results from the 18 *RXTE* observations, will be presented in separate papers. Of the remaining observations, in two cases the HETGS failed to insert, and in two other cases the source intensity was too faint for our graded, continuous-clocking observational mode to yield good spectra, but the source was clearly detected (for a good discussion of continuous clocking mode, see Marshall et al. 2001). The final *Chandra* observation was made when XTE J1550–564 was below 0.05 Crab, in timed exposure mode (to be presented in a separate paper).

The *RXTE* data we report here was obtained through pointed observations of the proportional counter array (PCA, Jahoda et al. 1996), which consists of five individual proportional counter units (PCUs). We combine “Standard 2” data from all layers of PCUs 1 and 4. The data was reduced using the standard LHEASOFT package (version 5.0). We apply the standard “goodtime” and detector “deadtime” corrections. The background was calculated using the “bright source” model within LHEASOFT. Following Miller et al. (2001), we use custom response matrices from PCA scientist Keith Jahoda, which are a better fit to the Crab spectrum in the iron line region, and use fits to the Crab to determine our fitting range and the appropriate systematic error. We find that the response matrices

achieve a satisfactory fit to the Crab with an additional systematic error of 1%. As the spectrum of XTE J1550–564 becomes background-dominated at energies above 40 keV, we fit the 3.0–40.0 keV range with 1% systematic errors added. Following Sobczak et al. 2000, we fix the neutral hydrogen column density ($N_{\text{H}} = 2.0 \times 10^{22} \text{ cm}^{-2}$). We analyze the *RXTE* data using the X-ray spectral fitting package XSPEC version 11.0 (Arnaud and Dorman 2000).

XTE J1550–564 was observed with the *Chandra* HETGS using the ACIS-S chips operating in continuous clocking (CC) mode. Because XTE J1550–564 had flared to 6.8 Crab (1.5–12 keV) during its 1998 outburst, avoiding damage to the ACIS array was a paramount concern. To this end, we employed a large dither (20" amplitude) to spread the most intense parts of the zeroth order over more pixels. Furthermore, the zeroth order aim point was shifted toward the top of the chip via a SIM-Z translation of +10.0mm from the nominal S3 aim point. A +1.33' Y-offset was used to place the iron K_{α} region of the HEG –1 order on ACIS-S3. Finally, we blocked-out rows 367–467, eliminating any read-out of zero-order photons. This blocking prevented damage to the chips, but also acted to limit any telemetry saturation that would result from the zero-order counts. The CC mode was employed to limit pile-up of the dispersed spectrum and to achieve 3 msec time resolution.

As our observing mode is non-standard, the data is not well-suited to reduction via the tools available in the CIAO suite. We have managed to build robust, custom software to reduce and analyze our data. We first correct for bad aspect times (e.g. slewing, see Table 1). The events are then examined in projected chip-x space to correct for “hot” pixels which report erroneously large event numbers (a list of bad pixels is available through CIAO). ACIS-S4 sometimes produces “streaks” which appear in the ACIS chip image (see <http://asc.harvard.edu>); the events were removed using a 50 column median filter, rejecting 3σ deviations. The spacecraft dither pattern is removed by calculating the mean chip-x position as a function of time, which is a sine wave.

We are able to interpolate the dither-corrected chip x position of each event by removing this sine wave. With the dither removed, it is possible to calculate the wavelength corresponding to each chip-x value via the grating equation. A linear gain correction is performed on each of the four independent read-out and amplifier nodes on each ACIS-S chip. Finally, we extract first-order MEG and HEG events and background regions, and apply the appropriate response matrices.

Indeed, although we have blocked-out the zero-order photons, we are able to accurately locate the position of the zero-order, and therefore able to convert accurately from chip x space to wavelength or energy space via the grating equation. To do this, we make use of the fact that the ACIS chips are silicon-based, and that silicon has an absorption edge at 1.8395 keV. For an assumed zero-order position, then, we can examine the location of this edge in the HEG +1 and HEG –1 spectra (which are on opposite sides of the zero-order position) and iterate the assumed zero-order position until the edge is seen at the same energy in both (see Figure 3).

For the purposes of this investigation of emission lines in the iron K_{α} region, we restrict our fits to the *Chandra* data to the 4.0–8.0 keV range. We set 4.0 keV as a lower bound as we expect a soft, thermal component to strongly dominate the spectrum below this energy. We set 8.0 keV as an upper bound because the source spectrum in the individual HEG orders becomes count-limited above this energy.

4. Results

Based on the ASM hardness ratio shown in Figure 1, and also on the continuum fit results (3.0–40.0 keV) shown in Figure 2, it is very likely that we have observed the IS. Fits to the *RXTE* data with a model consisting only of the multicolor disk blackbody plus power-law components are not formally acceptable ($\chi^2/(37 \text{ dof}) > 8$). The data/model ratio shows a broad excess in the iron K_{α} region (see Figure 2, panel B). Fits to the HS of the 1998 outburst of XTE J1550–564 with

this model are also unacceptable, and have a similar broad excess (Sobczak et al. 2000). Fits to the data using the “compTT” Comptonization code (Titarchuk 1994) in XSPEC were also very poor (again, $\chi^2/(37 \text{ dof}) > 8$) and gave a similar data/model ratio.

We add a Gaussian component to the model to improve our fit to the data. As we anticipate that any iron near to the central accretion environment in XTE J1550–564 is likely to be highly ionized due to the flux of the hard power-law, we fix the Gaussian centroid energy at 6.7 keV (helium-like Fe XXV $K_\alpha = 6.701 \text{ keV}$). The data are better fit by a broad feature (for R1, $\sigma = 1.26 \text{ keV}$; for R2, $\sigma = 1.47 \text{ keV}$) with large equivalent width ($\sim 800 \text{ eV}$). With the inclusion of the Gaussian feature, we obtain a formally acceptable fit to observation R2, and a marginally acceptable fit to observation R1; the parameters in both are tightly constrained (see Table 2). The multicolor disk blackbody temperatures and power-law indices we measure are consistent with observations of the VHS/IS in the 1998 outburst of XTE J1550–564 (Sobczak et al. 2000), but the Gaussian equivalent width we measure is much stronger than reported in the previous outburst. Based on tests using the standard F-statistic, the Gaussian in each fit is required at greater than 99.9% confidence. It should be noted that the fit to R1 can be improved by fitting a second Gaussian at 5.7 keV (see Figure 2, panel C). We are unable to constrain the parameters of any iron absorption edge when this component is included in the model.

After accounting for the instrumental response, we fit the *Chandra* data in the 4.0–8.0 keV range via a curve-fitting routine that minimizes χ^2 (the multi-variable minimization is done via the “AMOEBA” method; see Press, Teukolsky, Vetterling, and Flannery 1993). This is not as mathematically rigorous as folding a candidate spectrum through the instrument response function, and then minimizing χ^2 against the measured spectrum. However, this method is sound in the limit of an instrumental response that is a δ -function at every bin; the HETGS response approaches this limit.

We approximate the canonical model for BHGs by fitting a model consisting of a simple blackbody plus a power-law. The data do not constrain the power-law index tightly. As *RXTE* has a larger effective area and broader energy range, we fix the power-law index in fits to the *Chandra* data to the corresponding *RXTE*-measured value. With this constraint, the blackbody plus power-law model provides a formally acceptable fit to the data ($\chi^2/307 \text{ dof}=1.22$, C1; =1.26, C2). Although the models are different, it is worth noting that a blackbody temperature ($0.49 \text{ keV} \pm 5\%$, 90% confidence) is measured that is slightly below the color temperatures measured via the multicolor disk blackbody model in fits to the *RXTE* data. For the purpose of investigating lines in the iron K_α region, we only attempt a broadly correct characterization of the continuum emission, and leave an absolute flux comparison to future work.

We add a broad Gaussian to the model for each *Chandra* observation, fixed at 6.7 keV. The width of this added feature cannot be constrained by the data; we fix the width to the corresponding *RXTE*-measured value. This provides only a marginal improvement to the overall fit – the data in observations C1 and C2 only prefer the addition of this component at approximately 1σ . As the normalizations preferred by the data are consistent with zero at 1σ , we conclude that this component is not required.

To search for weak, narrow emission or absorption features in C1 and C2 (see Figure 4), we calculate the signal to noise ratio at each bin, which may be regarded as a lower limit on the significance of any deviation from the continuum. Following Cui et al. (2001), we identify a number of such features which are significant at 2σ , or greater. We find no features significant at 3σ . In the 4.0–8.0 keV range, we have 310 bins and therefore expect approximately 14 variations significant at 2σ , evenly split between positive and negative fluctuations. In C1, we find 16 features (9 positive, 6 negative) significant at 2σ , consistent with statistical fluctuation. We find 25 2σ features (13 positive, 12 negative) in observation C2. In the absence of any systematic errors, the

probability that this group of features is due to random variations would be 0.5%. However, given our lack of experience with this observation mode we suspect that they may be the result of some undocumented instrumental effect.

We note emission features in C1 at 6.68 keV and 7.02 keV that may be emission from Fe XXV and Fe XXVI (significant at 2.4σ and 2.2σ , respectively). We also note a feature at 5.76 keV, which may be emission from Ca XX (significant at 2.3σ). A similar feature may be seen in the *RXTE* data as well (see Figure 2, panel A). In C2, the only emission feature that might be associated with a known emission line at or near its laboratory value is at 6.73 keV (significant at 2.0σ), which may be due to Fe XXV. The prominent dip at 4.8 keV in both spectra is due to a chip gap, and is not a feature related to XTE J1550–564.

5. Discussion

BHCs observed in outburst with *RXTE* often require the inclusion of a broad Gaussian feature centered between 6.4 keV and 6.7 keV (e.g. Sobczak et al. 2000). In some cases, the parameters of the “diskline” or “Laor” emission line models – which describe the profile of a line produced in the inner accretion disk – can be constrained (Balucinska-Church & Church 2000, Miller et al. 2001). In fitting *RXTE* observations R1 and R2 (see Tables 1 and 2), we only attempt fits with a simple Gaussian fixed at 6.7 keV. The data strongly require a Gaussian of large equivalent width, that is very broad. A small feature remains at \sim 5.7 keV after we fit the broad Gaussian. The *Chandra* data allow but do not require a broad Gaussian at 6.7 keV with width fixed to the *RXTE* value. The inclusion of such a Gaussian in fits to the *Chandra* data gives a slight improvement to the fit, but the feature is not statistically significant.

These spectra are broadly consistent with those expected from highly ionized accretion disks (e.g. Ballantyne et al. 2001). Indeed, we measure a hard power-law flux in the 3.0–40.0 keV *RXTE* spectra

that could create a highly ionized inner accretion environment. A radio observation made on the same day as observations R2 and C2 finds no evidence for a jet (Corbel et al. 2001), likely eliminating a possible origin for these *Chandra* features. We speculate that a hot, optically-thin corona could produce weak, narrow spectral features consistent with our measurements.

We note that due to our short exposures, we have a low signal to noise ratio in our *Chandra* spectra. Confirmation of the presence of narrow spectral features (the majority of which may only be statistical noise in these observations), awaits future investigation with improved statistics. However, the lack of any strong narrow lines in the *Chandra* spectra may rule-out the possibility that the broad Gaussian required in the *RXTE* spectra is due to a collection of narrow lines. This may support the interpretation that the *RXTE* feature is an intrinsically (relativistically) broadened Fe K_{α} emission line.

6. Acknowledgments

We wish to acknowledge Harvey Tananbaum, Fred Seward, Jean Swank, Evan Smith, and the *Chandra* and *RXTE* operations staffs, for executing and coordinating these TOO observations. We thank *Chandra* scientist David Huenemoerder for sharing his analysis software expertise, and *RXTE*/PCA scientist Keith Jahoda for his generous help with the PCA detector response. We thank Ron Remillard, Michael Muno, and Chryssa Kouveliotou for numerous helpful discussions. W. H. G. L. gratefully acknowledges support from NASA. T. D. M. and R. W. were supported by NASA through Chandra fellowship grants PF9-10005 and PF9-10010, respectively, which are operated by the Smithsonian Astrophysical Observatory for NASA under contract NAS8-39073. This research has made use of the data and resources obtained through the HEASARC on-line service, provided by the NASA–GSFC.

REFERENCES

- Arnaud, K., and Dorman, B., 2000, XSPEC v. 11.0
- Ballantyne, D. R., Ross, R. R., and Fabian, A. C., 2001, MNRAS (accepted), astro-ph/0102040
- Balucinska-Church, M., and Church, M. J., 2000, MNRAS, 312, L55
- Blandford, R. D., & Begelman, M. C., 1999, MNRAS 303L, 1B
- Campbell-Wilson, D., McIntyre, V. Hunstead, R., Green, A., Wilson, R. B., & Wilson C. A., 1998 IAU Circ., 7010
- Chen, W., Shrader C. R., Livio, M., 1997
- Corbel, S., et al., 2001, ApJ, submitted
- Cui, W., et al. 2001, ApJ, 548, 394
- Ebisawa, K., et al., 1994 PASJ 46, 375-394
- Esin, A. A., McClintock, J. E., and Narayan, R., 1997, ApJ 489, 865
- Esin, A. A., McClintock, J. E., Drake, J. J., Garcia, M. R., Haswell, C. A., Hynes, R. I., and Munro, M., 2001, ApJ, in press
- Fabian, A. C., Rees, M. J., Stella, L., & White, N. E., 1989, MNRAS, 238, 729
- Fender, R. P., et al., 1999, MNRAS, 304, 865
- Fender, R. P., 2001, astro-ph/0101233
- George, I. M., & Fabian, A. C., 1991, MNRAS, 249, 352
- Homan, J., et al., 2001, ApJS, 132, 377-402
- Lee, J. C., et al. 2001, ApJL submitted, astro-ph/0101065
- Marshall, H. L., et al. 2001, AJ submitted, astro-ph/0103203
- Masetti, N., and Soria, R., 2000, IAU Circ., 7399
- Miller, J. M., et al., 2001, ApJ 546, 1055M
- Orosz, J. A. & Bailyn, C. D., 1997, ApJ, 477, 866
- Orosz, J. A., Bailyn, C., & Jain, R., 1998, IAU Circ., 7009
- Press, W. H., Teukolsky, S. A., Vetterling, W. T., and Flannery, B. P., 1993, “Numerical Recipes in C: The Art of Scientific Computing”, Cambr. Univ. Press, Cambridge, U. K.
- Remillard, R. A., Morgan, E. H., McClintock, J. E., Bailyn, C. D., & Orosz, J. A., 1999b, ApJ, 522, 397
- Shahbaz, T., van der Hooft, F., Casares, J., Charles, P. A., & van Paradijs, J., 1999, MNRAS, 306, 89
- Smith, D. A., 1998, IAU Circ., 7008
- Smith, D. A., Levine, A. M., Remillard, R. Fox, D., & Shaefer, R., 2000, IAU Circ., 7399
- Sobczak, G. J., et al. 1999, ApJ, 520, 766S
- Sobczak, G. J., et al. 2000, ApJ, 544, 993S
- Sunyaev, R. A. & Titarchuk, L. G., 1980, A & A, 86, 121
- Stella, L., Vietri, M., and Morsink, S. M., 1999, ApJ, 524, L63
- Tanaka, Y., et al., 1995, Nature, 375, 659
- Titarchuk, L, 1994, ApJ, 434, 314
- Tomsick, J. A., Smith, E., Swank, J., Wijnands, R., and Homan, J., 2001, IAU Circ., 7575

Table 1: Observation Log

No.	Obs.ID	Date, UT	Start Time	Day (year 2000)	Exp. (s)	Good Time (s)
C1	680	05/03/00	21:10:40	122.9	3380	2670
C2	681	05/06/00	12:54:09	125.5	3770	2170
R1	50134-02-04-00	05/03/00	16:33:20	122.7	4860	4860
R2	50134-02-06-00	05/06/00	12:50:08	125.5	3960	3960

Note. — These observations were made shortly after outburst maximum, during the “intermediate” X-ray state. “Good Time” is non-slewing observation time. C1 and C2 are the *Chandra* observations, R1 and R2 are the *RXTE* observations.

Table 2: *RXTE* Spectral Parameters

Obs. $\chi^2/(35 \text{ dof})$	T_{DBB} (keV)	N_{DBB} (E+3) [flux $_{3-40}$ (E-10)]	α_{pl}	N_{pl} [flux $_{3-40}$ (E-10)]	$\sigma_{6.7}$ (keV)	$N_{6.7}$ (E-3)	$\text{EW}_{6.7}$ (eV) [flux $_{3-40}$ (E-11)]
R1 1.80	0.73(1)	1.4(2) 9(1)	2.44(3)	0.66(6) 9.5 $^{+0.9}_{-0.7}$	1.26(8)	6.8 $^{+0.6}_{-0.5}$	783 $^{+62}_{-64}$ 7.0(6)
R2 1.08	0.78(2)	1.5(2) 16(2)	2.30(2)	0.99(6) 20(1)	1.47(7)	15(1)	839 $^{+71}_{-43}$ 15(1)

Note. — Results from spectral fits to *RXTE* observations R1 and R2. The full model consists of photoelectric absorption with $N_{\text{H}} = 2.0 \times 10^{22} \text{ cm}^{-2}$ fixed, the canonical multicolor disk blackbody and power-law components, and a Gaussian with centroid energy fixed at 6.7 keV. In both observations, the data requires the Gaussian for formally acceptable fits at greater than 99.9% confidence. Errors reported above are the parameter values at the 90% confidence limits. The 3–40 keV fluxes are reported in units of $\text{ergs cm}^2 \text{ s}^{-1}$.

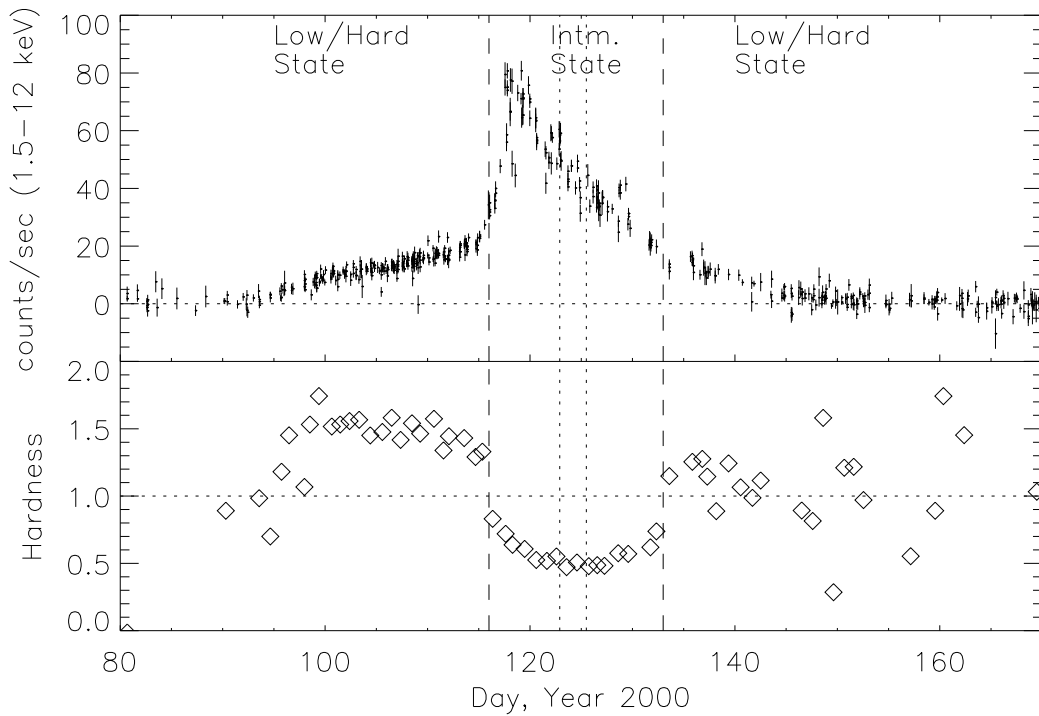


Fig. 1.— The ASM 1.5-12 keV lightcurve and $(5-12 \text{ keV})/(3-5 \text{ keV})$ count-rate ratio for the April-May 2000 outburst of XTE J1550–564. Dotted vertical lines indicate the approximate start times of our *Chandra* observations. Dashed vertical lines separate X-ray states. State identifications based on the ASM hardness ratio, and radio observations reported by Corbel et al. (2001)

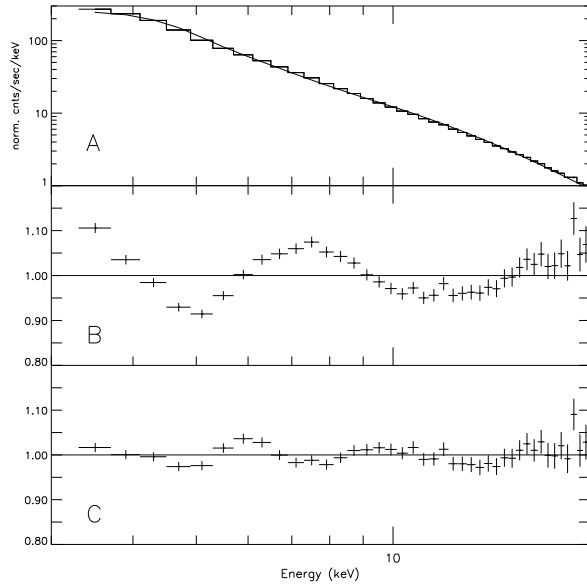


Fig. 2.— The 3–20 keV spectrum and data/model ratios for two models fit to observation R1. Though we fit the 3–40 keV range, we show only the 3–20 keV range here to emphasize the iron line region. Models include photoelectric absorption fixed at $N_{\text{H}} = 2.0 \times 10^{22} \text{ cm}^{-2}$. A: The R1 spectrum fit with a model consisting of the multicolor disk blackbody plus a power-law. B: The data/model ratio for this model – an unacceptable fit ($\chi^2/(35 \text{ dof}) = 8.64$). C: The data/model ratio for a model with a Gaussian fixed at 6.7 keV ($\chi^2/(35 \text{ dof}) = 1.80$). The panels shown here are similar for observation R2. The fit to R1 only is further improved if a second Gaussian is fit at 5.7 keV.

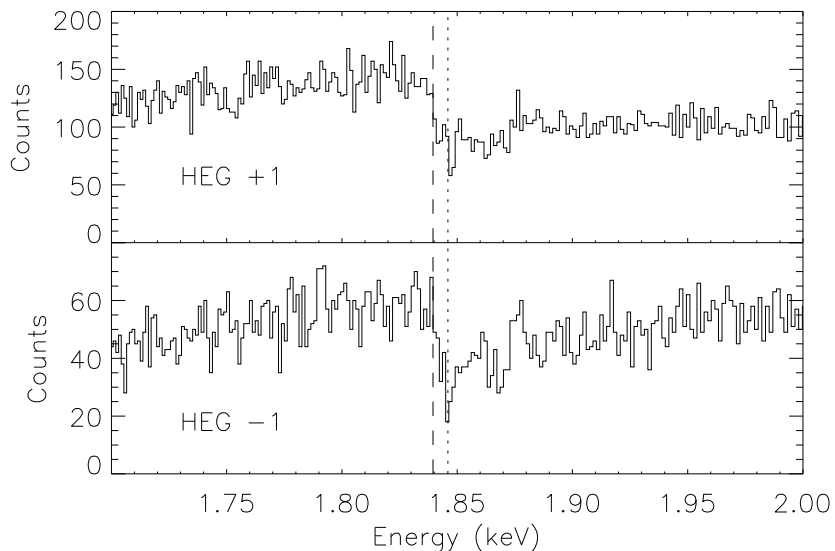


Fig. 3.— The count spectrum of XTE J1550–564 near the instrumental silicon absorption edge. The dashed line is the laboratory edge energy (1.8395 keV). The dotted line is the edge minimum, which we can align to within the instrumental resolution. This provides an effective means of establishing the zeroth-order position, and therefore energy as a function of position on the ACIS-S array. This is necessary as we blocked the zeroth-order photons with a spatial window to prevent telemetry saturation.

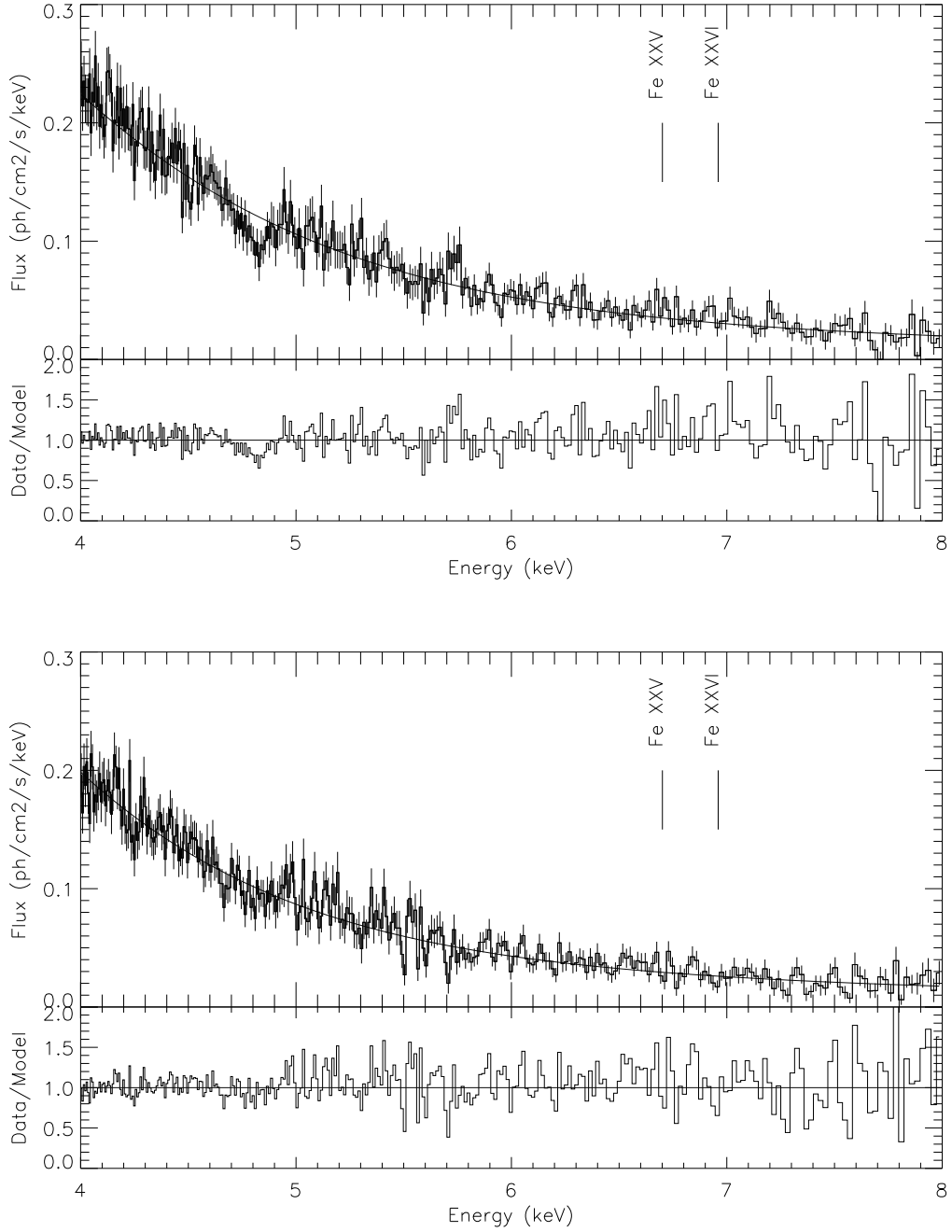


Fig. 4.— Combined HEG first-order 4–8 keV spectrum from C1 (above) and C2 (below). Only a simple blackbody plus power-law model with α_{pl} fixed to the *RXTE*-measured value is fit to characterize the continuum. The data/model ratio is shown below each spectrum. For convenience, we identify the rest-frame energies of helium-like and hydrogenic iron.